Dalton Transactions

Accepted Manuscript

This article can be cited before page numbers have been issued, to do this please use: A. Sarkar, C. Loho, L. Velasco, T. Thomas, S. S. Bhattacharya, H. Hahn and R. R. Djenadic, *Dalton Trans.*, 2017, DOI: 10.1039/C7DT02077E.




ROYAL SOCIETY OF CHEMISTRY

rsc.li/dalton

View Article Online
DOI: 10.1039/C7DT02077E

# Multicomponent equiatomic rare earth oxides with narrow band gap and associated praseodymium multivalency

*Abhishek Sarkar,*[1,2] Christoph Loho,[2] Leonardo Velasco,[1] Tiju Thomas,[3] Subramshu S. Bhattacharya,[3] Horst Hahn, *[1,2,4] and Ruzica Djenadic[2,4,†]*

[1]Institute of Nanotechnology, Karlsruhe Institute of Technology, Hermann-von-Helmholtz-Platz 1, 76344 Eggenstein-Leopoldshafen, Germany

[2]Joint Research Laboratory Nanomaterials – Technische Universität Darmstadt and Karlsruhe Institute of Technology, Alarich-Weiss-Str. 2, 64287 Darmstadt, Germany

[3]Department of Metallurgical and Materials Engineering, Indian Institute of Technology Madras, Chennai-600036, India

[4]Helmholtz Institute Ulm – Electrochemical Energy Storage, Helmholtzstr. 11, 89081 Ulm, Germany

*Corresponding author: abhishek.sarkar@kit.edu, horst.hahn@kit.edu

[†]Present address: Heraeus Deutschland GmbH & Co. KG, Heraeusstr. 12 – 14, 63450 Hanau, Germany.

**KEYWORDS**: nanocrystalline, visible light absorption, oxygen defects, UV-Vis spectroscopy, Raman spectroscopy

View Article Online
DOI: 10.1039/C7DT02077E



**ABSTRACT:**

New multicomponent equiatomic rare earth oxides (ME-REOs) containing 3 – 7 rare earth elements (Ce, Gd, La, Nd, Pr, Sm and Y) in equiatomic proportions are synthesized using nebulized spray pyrolysis. All the systems crystallized as phase pure fluorite type ($Fm\bar{3}m$) structure in spite of the high chemical complexity. Nominal increase in lattice parameter compared to $CeO_2$ is observed in all ME-REOs. X-ray photoelectron spectroscopy performed on the ME-REOs confirmed that all the constituent rare earth elements are present in 3+ oxidation state, except for Ce and Pr which are present in 4+ and in a mixed (3+/4+) oxidation state, respectively. The presence of $Ce^{4+}$ contributes substantially to the observed stability of the single phase structure. These new oxide systems have narrow direct band gaps in the range of 1.95 – 2.14 eV and indirect band gaps in the range of 1.40 – 1.64 eV, enabling light absorption over the entire visible spectral range. Furthermore, the oxygen vacancies concentration rapidly increases and then saturates with the number of rare earth elements that are incorporated in ME-REOs. The lowering of the band gap is found to be closely related to the presence of multivalent Pr. Interestingly, the band gap values are relatively invariant with respect to composition or thermal treatments. Considering the high level of oxygen vacancies present and the observed low band gap values, these new material systems can be of importance where the presence of oxygen vacancies is essential or in applications where narrow band gap is desirable.

**Electronic supplementary information.** Table containing the details of Rietveld refinements, table and graphs showing variation of lattice parameters with respect to cationic radii, XRD patterns and Tauc plots for ME-REO systems without Pr are provided in the supplementary information file.

View Article Online
DOI: 10.1039/C7DT02077E



## 1. INTRODUCTION

Materials shape our world and discoveries of new ones create novel opportunities and challenges. Recently, a group of researchers[1] decided to deviate from the conventional binary or doped oxides and pioneered the field of multicomponent equiatomic oxides (MEOs). This new class of materials is also known as entropy stabilized oxides due to the high configurational entropy of the systems, caused by the presence of multiple cations in equiatomic amounts. These oxides show interesting transport properties[2,3] and can be obtained by different synthesis methods.[4,5] Until the discovery of MEOs, the idea of multicomponent equiatomic systems had more or less been limited to random solid solutions in metals known as high entropy alloys (HEAs).[6] It has been recently shown that the concept of MEOs is not only limited to transition metal based oxides,[1] but can be extended to rare earth based oxides as well.[7] In these new multicomponent equiatomic rare earth oxides (ME-REOs), up to seven different rare earth cations (predominantly in the 3+ oxidation state) can be mixed in equiatomic amounts (unlike doping) and successfully accommodated into a single-phase fluorite ($Fm\bar{3}m$) type structure. This result is fascinating considering the fact that except for $CeO_2$ and $PrO_2$, all the binary oxides of the remaining constituent rare earth elements have crystal structures other than fluorite. Furthermore, the oxides of the constituent rare earth elements are not completely miscible (at equiatomic ratio) according to their binary phase diagrams.[8] It has also been found that unlike the entropy dominated structure stabilization, as observed in case of transition metal based MEOs,[1] the presence of Ce in 4+ oxidation state determines the stability of single phase in the ME-REOs. This has been confirmed by the fact that all the ME-REO systems without Ce are not phase pure, regardless of the thermal treatment performed.[7] The study[7] has not only extended the broad spectrum of research on multicomponent oxide systems but also added a fresh insight by

View Article Online
DOI: 10.1039/C7DT02077E



demonstrating that factors other than entropy can be used to stabilize simple structures and design new multicomponent material systems.

For several decades, rare earths oxides have been known for their interesting optical, electronic and chemical properties. They have been deployed in a wide range of applications such as phosphors, sunscreen cosmetics, magneto-optical devices, catalysts, biomarkers, colorants for special glasses, solid electrolytes, etc.[9] Each of these fields, in principle, may be influenced by ME-REOs owing to the cumulative effect of multiple RE cations. Out of the many rare earth oxides, ceria ($CeO_2$) has been widely studied due to its wide band gap and non-stoichiometry. The observed non-stoichiometry arises from the presence of oxygen vacancies making ceria an excellent material for UV light blockers, gas sensors, oxygen storage capacitors, catalysts and solid oxide fuel cells.[9–11] Several studies[12,13] have also focused on engineering the band gap of ceria in order to make it active in the visible light range. Making a material photoactive in the visible region leads to possibilities such as use in photocatalytic applications.[14,15]

In this investigation, we follow-up on our previous article on ME-REOs,[7] introducing high resolution transmission electron microscopy (HR-TEM) and spectroscopic studies like X-ray photoelectron spectroscopy (XPS), UV-Vis spectroscopy and Raman spectroscopy in order to gain a deeper understanding of the structure and properties of these newly discovered materials. Information about the defect structure of these materials and its effect on their band gap is extracted from the combined spectroscopic studies.

View Article Online
DOI: 10.1039/C7DT02077E



## 2. EXPERIMENTAL SECTION

**2.1. Powder synthesis**. ME-REOs containing 3 – 7 rare earth cations (Ce, Gd, La, Nd, Pr, Sm, Y) in equiatomic amounts are synthesized from water-based solutions of rare earth nitrates using nebulized spray pyrolysis (NSP). $CeO_2$ and a binary cation system, $(Ce_{0.5}Pr_{0.5})O_2$, which are the reference systems, are synthesized using the same technique. The powders are further calcined at 1000 °C for 1 hour in air to study the effect of thermal treatment on the crystal structure and the optical properties. The detailed description of the experimental setup and synthesis procedure are reported in our previous study.[7]

**2.2. Powder characterization**. The room temperature X-ray diffraction (XRD) patterns are recorded using a Bruker D8 Advance diffractometer with Bragg-Brentano geometry equipped with an X-ray tube with a Cu anode and a Ni filter. The Rietveld refinements are done using TOPAS 5[16] to gain information about the lattice parameters, phase compositions, crystallite sizes and lattice strains. The detailed description of the refinement parameters are previously reported.[7]

Specimens for transmission electron microscopy (TEM), from the as-synthesized and calcined powders, are prepared by directly dispersing the finely ground powders onto a standard carbon coated copper grid. A Philips Technai F20 ST electron microscope (operating at 200 kV) is used to examine the specimens.

Oxidation states of all elements in representative samples of as-synthesized and calcined system, $(Ce_{0.2}La_{0.2}Pr_{0.2}Sm_{0.2}Y_{0.2})O_{2-\delta}$, are determined using XPS, that is performed using a PHI 5000 spectrometer equipped with a monochromatic Al Kα excitation source. A charge neutralizer with low-energy electrons is used to compensate and minimize charging effects in the investigated oxides.

View Article Online
DOI: 10.1039/C7DT02077E



The UV-Vis spectra are recorded in the range from 200 nm to 1200 nm using a Perkin-Elmer Lambda 900 spectrophotometer. From the obtained spectra, optical band gaps are determined by applying the Tauc relation:[17]

$$[F(R_\infty)\cdot h\nu]^{1/n} = A\cdot(h\nu - E_g) \quad (1)$$

where $F(R_\infty)$ is the Kubelka-Munk function, $h$ is the Planck's constant, $\nu$ is the vibrational frequency, $A$ is a constant, and $E_g$ is the band gap energy. The exponent $n$ denotes the nature of the optical transitions. The values of $n$ = ½ and $n$ = 2 are used for direct and indirect allowed transitions, respectively. The band gap (direct and indirect) energy values are calculated from linear regression at the inflection point of the $[F(R_\infty)\cdot h\nu]^{1/n}$ vs. $h\nu$ (Tauc) plots. The obtained $h\nu$-intercept values are taken as the band gap values.

The Raman spectra are recorded with a confocal micro-Raman spectrometer, Horiba Jobin Yuvon HR 800, using a 633 nm He-Ne laser in the range of 300 – 1000 $cm^{-1}$. All the spectra are the result of 40 accumulations, each lasting 20 s.

## 3. RESULTS AND DISCUSSION

**3.1 XRD and TEM studies**. Figure 1 shows the X-ray diffraction (XRD) patterns for the as-synthesized (Figure 1a) and calcined (Figure 1b) powders. In our previous study,[7] the detailed structural analyses confirmed that the as-synthesized systems with 3 to 6 rare earth cations crystallize into a single phase fluorite ($Fm\bar{3}m$) type structure. The volume-weighted mean crystallite sizes of the ME-REOs (ranging from 7 nm to 10 nm) are obtained from the Rietveld analysis of the XRD patterns using TOPAS 5.[16] A small amount (~ 3 wt.%) of secondary phase ($La_2O_3$ prototype), alongside the main fluorite type phase, is formed in case of the 7 component system. The possible reason for formation of the secondary phase can be the sluggish diffusion

View Article Online
DOI: 10.1039/C7DT02077E



due to the increased number of cations, which are competing for the same position in the crystal lattice.[7] An increase in the lattice parameter compared to that of the $CeO_2$ (see Supplementary Information, Table S1) is observed for all the ME-REOs. The reason for lattice expansion is closely related to the oxidation state of the constituent cations and hence, explained in section 3.3.

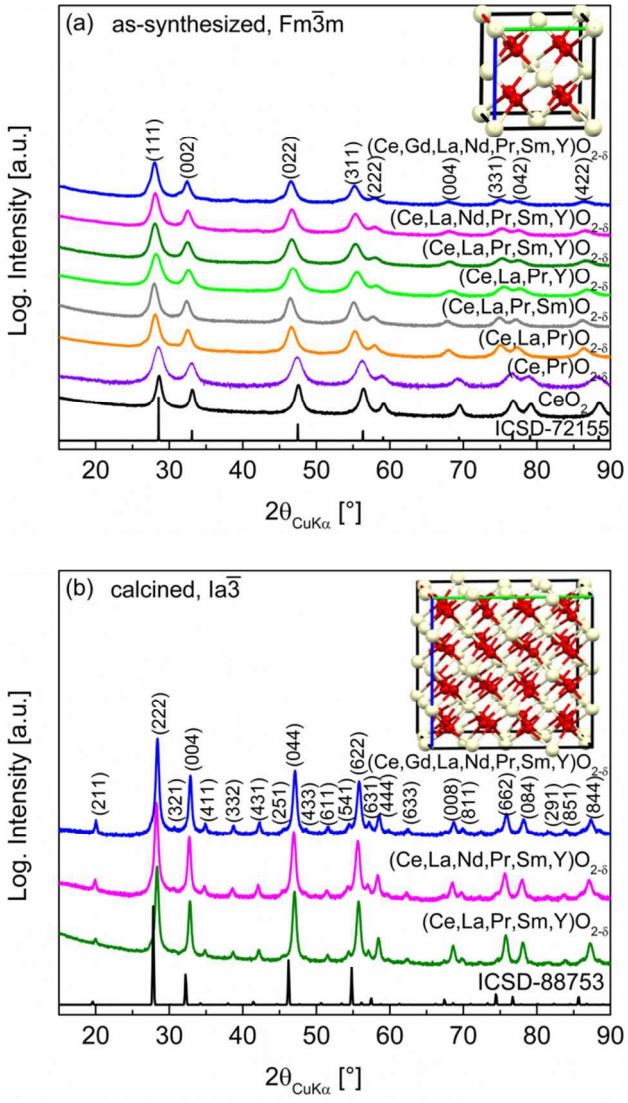


**Figure 1.** XRD patterns of (a) as-synthesized, $Fm\bar{3}m$ and (b) calcined, $Ia\bar{3}$ ME-REO powders confirming their phase purity. The ICSD patterns are simulated patterns of $Fm\bar{3}m$ (ICSD-72155) and $Ia\bar{3}$ (ICSD-88753) structures.

View Article Online
DOI: 10.1039/C7DT02077E



Based on the structure, the general formula for ME-REOs is chosen to be $(RE)O_{2-\delta}$, where RE depends on the type and the number of elements (in equiatomic amounts) present in their alphabetical order. For instance, the sample containing five RE elements, e.g., Ce, La, Pr, Sm, and Y, is labeled as $(Ce,La,Pr,Sm,Y)O_{2-\delta}$ indicating that all five cations are present in equiatomic amounts, i.e., $(Ce_{0.2}La_{0.2}Pr_{0.2}Sm_{0.2}Y_{0.2})O_{2-\delta}$. The reason for the oxygen non-stoichiometry is discussed in detail in section 3.2. Upon calcination at 1000 °C, the as-synthesized powders undergo a lowering of the crystal symmetry from the fluorite ( $Fm\bar{3}m$ ) to a bixbyite ( $Ia\bar{3}$ ) type structure (a body centered subgroup of $Fm\bar{3}m$ ). This is evident from the additional superstructure reflections (like (211), (321), (431), etc.) observed in the XRD patterns (Figure 1b) of the calcined powders. No signature of a secondary/impurity phase is observed in any of the calcined systems (see Supplementary Information Table S1). The mean crystallite sizes in the calcined powders are larger than that of the as-synthesized ones, but still remain in the nanometer range (29 – 34 nm).

HR-TEM imaging is performed on the as-synthesized and calcined $(Ce,La,Pr,Sm,Y)O_{2-\delta}$ powders, which are taken as representatives for all the systems. Both as-synthesized and calcined samples are highly crystalline with well-defined lattice fringes that are observed for most of the particles (Figure 2 (a) and (b)). The lattice parameters of both as-synthesized and calcined powders obtained from the selected area diffraction (SAED) patterns (Figure 2 (c) and (d)) are in good agreement with the results obtained from the Rietveld refinements (see Supplementary Information Table S1). In case of the calcined samples, additional weak diffraction rings corresponding to the less intense superstructure reflections ((211), (431), etc.) for the lower symmetry ( $Ia\bar{3}$ ) structure are observed in the SAED pattern (Figure 2d). These weak diffraction rings are absent in the SAED pattern for as-synthesized powder (Figure 2c), having the higher

View Article Online
DOI: 10.1039/C7DT02077E



symmetry fluorite ($Fm\bar{3}m$) type structure. These results are in good agreement with the previously discussed XRD results.

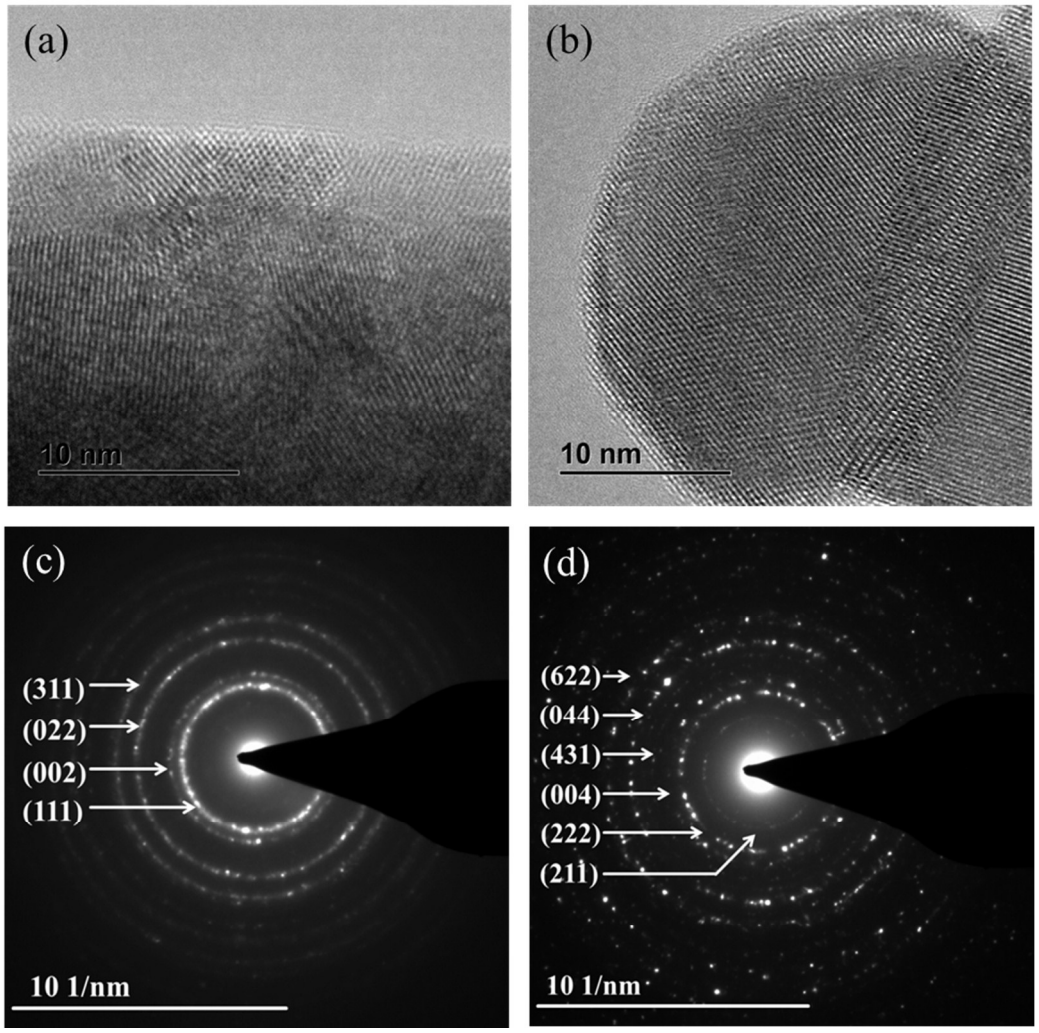


**Figure 2**. HR-TEM micrographs (a,b) and SAED patterns (c,d) for as-synthesized and calcined (Ce,La,Pr,Sm,Y)$O_{2-\delta}$ powders, respectively. The TEM results are in good agreement with the XRD results.

**3.2 XPS studies**. The oxidation states of the elements present in the as-synthesized as well as in the calcined (Ce,La,Pr,Sm,Y)$O_{2-\delta}$ powders are determined using XPS analysis. The XPS spectra of the calcined (Ce,La,Pr,Sm,Y)$O_{2-\delta}$ powder (Figure 3) are identical to those obtained from the as-synthesized sample, ruling out any change in oxidation states during calcination. In

View Article Online
DOI: 10.1039/C7DT02077E

the La 3*d* spectra two doublets, at around 834 and 850 eV, are observed, which indicate the presence of $La^{3+}$, and is in good agreement with the reported literature results.[18] Two bands corresponding to $3d_{5/2}$ and $3d_{3/2}$ are observed in 3*d* spectra of Sm at around 1080 eV and 1110 eV, respectively. These bands indicate the presence of Sm in 3+ oxidation state.[19]

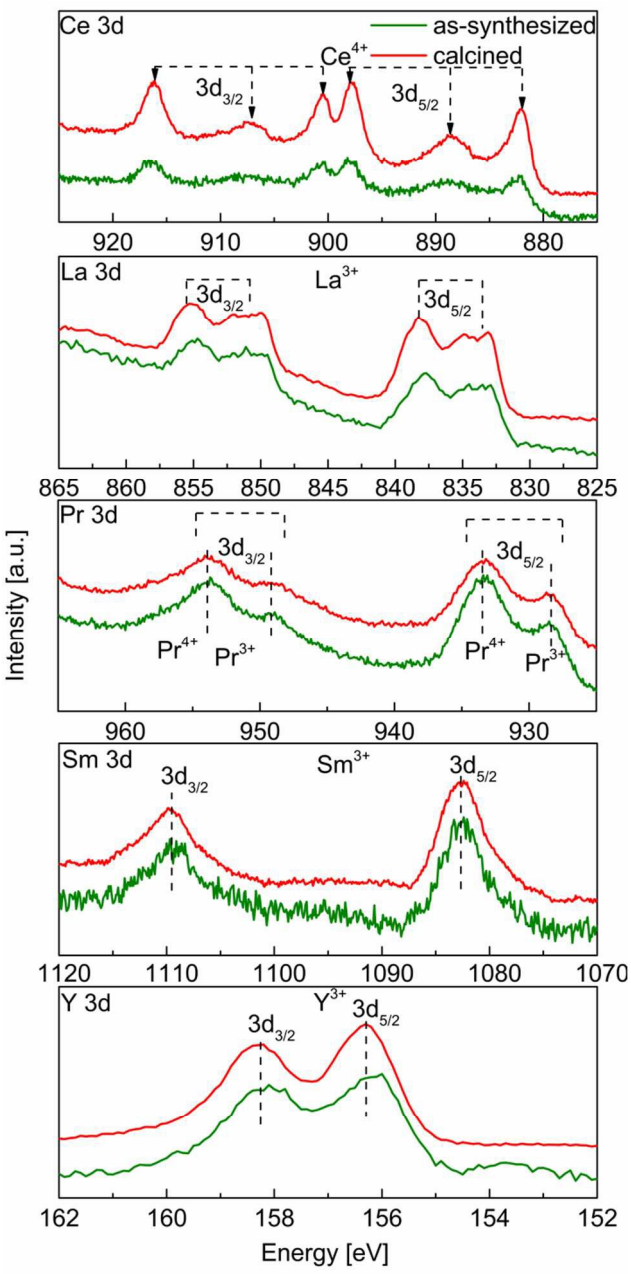


**Figure 3**. XPS spectra of as-synthesized and calcined $(Ce,La,Pr,Sm,Y)O_{2-\delta}$ powders as representatives of $(RE)O_{2-\delta}$ systems showing no effect of calcination on the oxidation states of RE elements.

View Article Online
DOI: 10.1039/C7DT02077E



The 3*d* spectra of Y are in agreement with those reported in literature[20] confirming that Y is present in the 3+ oxidation state. Unlike other lanthanide atoms (present in ME-REOs), Ce and Pr are often associated with multiple oxidation states (i.e., 3+ and 4+). The reason for this is their electronic configuration and the related in-situ redox reaction between their 3+ and 4+ oxidation states.[21] In case of Ce, the 4+ ($4f^0$) state is more stable than $Ce^{3+}$ ($4f^1$). In ME-REOs, Ce is found to be present in the 4+ oxidation state. This is because its 3*d* spectra show three distinct doublets similar to the ones observed for $Ce^{4+}$ in $CeO_2$.[22] $Ce^{4+}$ is found to contribute substantially to the stabilization of the single phase in ME-REOs. This is evidenced by the fact that the ME-REO systems without Ce are not phase pure, regardless of the number of RE elements present or the thermal treatment performed.[7] However, presence of minor amount of $Ce^{3+}$ cannot be excluded. In case of Pr ($4f^3\ 6s^2$), the possibility of a mixed (3+ and 4+) oxidation state is higher than that in Ce.[21] The 3*d* spectra of Pr in ME-REOs indicate the multivalent state of Pr owing to its close resemblance to that of $Pr_6O_{11}$.[23,24] Also the XRD pattern of the pure Pr-oxide (synthesized using the same method under similar conditions) matched the one of $Pr_6O_{11}$ closely rather than $PrO_2$ or $Pr_2O_3$.[7] Additionally, the linear fitting of the variation in the lattice parameters with respect to the average cationic radii (see Supplementary Information, Figure S1 and the related discussion), for different ME-REOs, indicates the presence of a mixed valence state of Pr (with the ratio of $Pr^{3+}$ to $Pr^{4+}$ close to that in $Pr_6O_{11}$). The presence of higher amount of $Pr^{4+}$ is also in good agreement with literature[25] where it is observed that the existence of $Pr^{4+}$ is often favored by the presence $Ce^{4+}$ and other $RE^{3+}$ cations in the system. The oxidation states of the RE elements in the other ME-REOs (reported here) are the same as in the $(Ce,La,Pr,Sm,Y)O_{2-\delta}$, as similar experimental (synthesis/calcination) conditions are used for all the systems. The presence of the elements in

View Article Online
DOI: 10.1039/C7DT02077E



both 3+ and 4+ oxidation states, justifies the selection of the general non-stoichiometric formula, $(RE)O_{2-\delta}$, for ME-REOs.

**3.3. UV-Vis spectroscopy**. The ultraviolet-visible (UV-Vis) absorption spectra for all as-synthesized $(RE)O_{2-\delta}$ systems (Figure 4a) are similar, exhibiting strong absorption below 650 nm, which is consistent with the dark brown color of the powders (see inset in Figure 4a). On the other hand, pure $CeO_2$, synthesized under similar conditions as a reference for $(RE)O_{2-\delta}$ , is pale yellow and exhibits strong absorption only below 450 nm. The absorption spectra for the calcined systems (Figure 4b) are very similar to those of the as-synthesized ones, indicating that symmetry lowering has minimal effect on the optical properties of these systems. In both as-synthesized as well as calcined systems containing Sm and Nd, several distinct absorption bands in the region from 750 nm to 1100 nm are observed. The prominent absorption bands found at 750 nm, 815 nm and 885 nm are related to the transition from the $4f^N$ ground state to the excited-state of $Nd^{3+}$ ion ($^4I_{9/2} \rightarrow {}^4F_{7/2}$, $^4S_{3/2}$), ($^4I_{9/2} \rightarrow {}^4F_{5/2}$, $^2H_{9/2}$), and ($^4I_{9/2} \rightarrow {}^4F_{3/2}$),[26] respectively. The absorption band in the infrared region (at 1080 nm) is related to the $^6H_{5/2} \rightarrow {}^6F_{9/2}$ transition of the $Sm^{3+}$ ion.[27] Based on these findings and XPS results, following conclusion regarding the oxidation states of the RE atoms in the ME-REOs can be drawn: $Ce^{4+}$, $Gd^{3+}$, $La^{3+}$, $Nd^{3+}$, $Sm^{3+}$, $Y^{3+}$ and Pr in mixed 3+ and 4+ states. The observed oxidation states can explain the expansion of the crystal lattice of ME-REOs compared to that of ceria as mentioned in section 3.1., i.e., the substitution of smaller $Ce^{4+}$ (0.94 Å) by other larger rare earth cations like $Gd^{3+}$ (1.05 Å), $La^{3+}$ (1.16 Å), $Nd^{3+}$ (1.10 Å), etc., in ME-REOs. The linear variation of the lattice parameters as a function of average cationic radii (see Supplementary Information, Figure S1b and related discussion), for different ME-REOs, follows the Vegard's law.[28]

View Article Online
DOI: 10.1039/C7DT02077E



Band gap values of ME-REO systems are determined from Tauc plots, $[F(R_\infty)\cdot h\nu]^{1/n}$ vs. $h\nu$, using the procedure described in the experimental section. Figure 4c and 4d display the Tauc plots only for the as-synthesized and calcined (Ce,La,Pr,Sm,Y)$O_{2-\delta}$ systems (which are the representative samples).

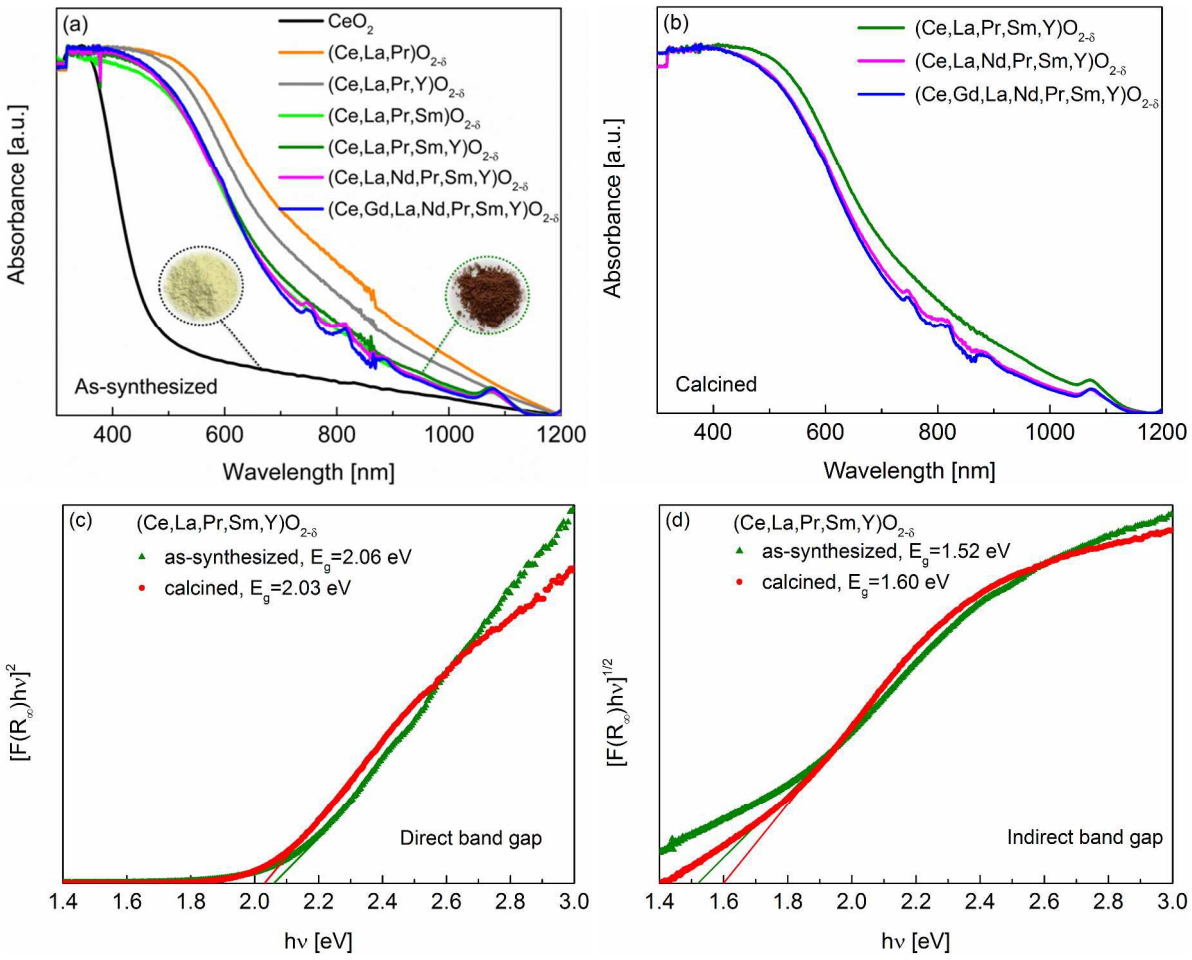


**Figure 4.** UV-Vis absorption spectra of (a) as-synthesized and (b) calcined (RE)$O_{2-\delta}$ powders showing strong absorption in the visible light region unlike $CeO_2$ powder. Insets in (a) show the colors of the as-synthesized powders. Tauc plots, $[F(R_\infty)\cdot h\nu]^{1/n}$ vs. $h\nu$, of as-synthesized and calcined (Ce,La,Pr,Sm,Y)$O_{2-\delta}$ systems with $n$ = ½ for direct band gap (c) and $n$ = 2 for indirect band gap (d) determination.

The direct band gap values (Figure 4c) are found to be 2.06 eV and 2.03 eV for the as-synthesized and calcined (Ce,La,Pr,Sm,Y)$O_{2-\delta}$ samples, respectively. The indirect band gap

View Article Online
DOI: 10.1039/C7DT02077E



values (Figure 4d) are even lower: 1.52 eV for the as-synthesized and 1.60 eV for the calcined powders. As the electronic structure of ME-REOs is unknown, both direct and indirect band gap values for all the ME-REO systems (as-synthesized and calcined) are calculated and reported in Table 1. However, for further discussion only the direct band gap values are considered. This decision is made based on reports pertaining to $CeO_2$, which can be considered as the parent structure of ME-REOs (owing to their structural similarities). Even though the electronic structure of $CeO_2$ is still being debated and both direct as well as indirect band gap values are often reported,[29,30] it is believed[31,32] that direct rather than indirect transitions take place in ceria.

**Table 1**. Summary of direct and indirect band gap energy ($E_g$) values (in eV) of as-synthesized ( $Fm\bar{3}m$ ) and calcined ( $Ia\bar{3}$ ) $(RE)O_{2-\delta}$ powders.

| Systems | Direct $E_g$ | Indirect $E_g$ |
|---|---|---|
| As-synthesized, $Fm\bar{3}m$ | | |
| $CeO_2$ | 3.17 | 2.76 |
| $(Ce,La,Pr)O_{2-\delta}$ | 1.95 | 1.42 |
| $(Ce,La,Pr,Y)O_{2-\delta}$ | 1.98 | 1.50 |
| $(Ce,La,Pr,Sm)O_{2-\delta}$ | 2.14 | 1.56 |
| $(Ce,La,Pr,Sm,Y)O_{2-\delta}$ | 2.06 | 1.52 |
| $(Ce,La,Nd,Pr,Sm,Y)O_{2-\delta}$ | 2.12 | 1.62 |
| $(Ce,Gd,La,Nd,Pr,Sm,Y)O_{2-\delta}$ | 2.11 | 1.64 |
| Calcined, $Ia\bar{3}$ | | |
| $(Ce,La,Pr,Sm,Y)O_{2-\delta}$ | 2.03 | 1.60 |
| $(Ce,La,Nd,Pr,Sm,Y)O_{2-\delta}$ | 2.06 | 1.56 |
| $(Ce,Gd,La,Nd,Pr,Sm,Y)O_{2-\delta}$ | 2.08 | 1.58 |

It can be observed from Table 1 that the band gap values are similar for both the as-synthesized and the calcined ME-REO systems (in the range 1.98 – 2.14 eV) and are also relatively independent of the number of RE elements. Clearly, the change in the structure during calcination, i.e., the lowering of symmetry from $Fm\bar{3}m$ to $Ia\bar{3}$ has no significant influence on the optical response of the $(RE)O_{2-\delta}$ systems. This offers substantial compositional as well as

View Article Online
DOI: 10.1039/C7DT02077E



structural flexibility without compromising their visible light absorption capabilities, which could be of importance for their practical applications. The most interesting result is that the band gap values (both direct and indirect) of ME-REOs are significantly lower when compared to the band gap values of any of the binary rare earth oxides or even many of the doped rare earth oxides.[30,33–37]

**3.4. Raman spectroscopy**. Oxygen vacancies are frequently associated with band gap narrowing in many oxides, including $CeO_2$.[32] Therefore, considering a perfect fluorite structure, like $CeO_2$, the presence of oxygen defects could be the possible reasons for the observed band gap narrowing in $(RE)O_{2-\delta}$. The formation of oxygen vacancies in ME-REOs can be attributed to the fact that except for $Ce^{4+}$ and $Pr^{3+/4+}$, all other rare earth cations are present in the 3+ oxidation state. In order to maintain the charge balance, oxygen vacancies ($V_O^{\bullet\bullet}$) are created according to the following defect formation reaction written in Kröger–Vink notation ($M_{RE}^{'}$ - $RE^{3+}$ on $RE^{4+}$ site; $O_O^{\times}$ - oxygen on oxygen site, no charge):

$$M_2O_3 \xrightarrow{(RE)O_2} 2M_{RE}^{'} + 3O_O^{\times} + V_O^{\bullet\bullet} \qquad (2)$$

As all cations are in equiatomic proportions, the concentration of oxygen vacancies is much higher than in any of the doped or non-stoichiometric binary rare oxides. In order to understand if the oxygen vacancies could be responsible for this significant band gap lowering, the amounts of the oxygen vacancies are estimated using the following considerations: (i) the $RE^{3+}$ and $RE^{4+}$ exclusively form $(RE)_2O_3$ and $(RE)O_2$, respectively, where oxygen stoichiometry ($x$) in $(RE)_2O_3$ is 1.5 and in $(RE)O_2$ is 2; and (ii) $(RE)O_{2-\delta}$ systems contain RE elements in both 3+ and 4+ oxidation states ($Ce^{4+}$, $Gd^{3+}$, $La^{3+}$, $Nd^{3+}$, $Pr^{4+/3+}$, $Sm^{3+}$, and $Y^{3+}$). Thus, the oxygen stoichiometry in $(RE)O_{2-\delta}$ can then be expressed as:

View Article Online
DOI: 10.1039/C7DT02077E

$$x = 1.5 \cdot \left[RE^{3+}\right] + 2 \cdot \left[RE^{4+}\right] \quad (3)$$

where $[RE^{3+}]$ and $[RE^{4+}]$ are the molar fractions of RE cations in 3+ and 4+ oxidation states, respectively. Therefore, the deviation from stoichiometry, i.e., the amount of oxygen vacancies ($\delta$) can be estimated from:

$$\delta = 2 - x \quad (4)$$

Table 2 gives an overview of the level of oxygen vacancies calculated based on the XPS/UV-Vis results according to the Equations 3 and 4. From table 2 it is clear that the oxygen defect concentration increases as the number of RE cations in 3+ oxidation state increases. Therefore, Raman spectroscopy is performed on the systems for further investigation of the oxygen vacancies due to its high sensitivity towards lattice defects.

**Table 2**. Overview of the estimated level of oxygen vacancies ($\delta$) in the as-synthesized powders based on Equation 3 and 4. The $[RE^{3+}]$ and $[RE^{4+}]$ represent the molar fractions of RE in 3+ and 4+ oxidation states, respectively, and $x$ represents oxygen stoichiometry.

| Systems, $Fm\bar{3}m$ | $[RE^{3+}]$ | $[RE^{4+}]$ | $x$ | $\delta$ |
|---|---|---|---|---|
| $CeO_2$ | 0.00 | 1.00 | 2 | 0 |
| $(Ce,Pr)O_{2-\delta}$ | 0.17 | 0.83 | 1.92 | 0.08 |
| $(Ce,La,Pr)O_{2-\delta}$ | 0.45 | 0.55 | 1.78 | 0.22 |
| $(Ce,La,Pr,Y)O_{2-\delta}$ | 0.50 | 0.50 | 1.71 | 0.29 |
| $(Ce,La,Pr,Sm)O_{2-\delta}$ | 0.50 | 0.50 | 1.71 | 0.29 |
| $(Ce,La,Pr,Sm,Y)O_{2-\delta}$ | 0.60 | 0.40 | 1.67 | 0.33 |
| $(Ce,La,Nd,Pr,Sm,Y)O_{2-\delta}$ | 0.67 | 0.33 | 1.64 | 0.36 |
| $(Ce,Gd,La,Nd,Pr,Sm,Y)O_{2-\delta}$ | 0.72 | 0.28 | 1.62 | 0.38 |

The Raman spectra, obtained using a He-Ne laser source ($\lambda$ = 633 nm), for different ME-REOs are shown in Figure 5. For $CeO_2$ a single sharp band at 464 $cm^{-1}$ is observed. This band is

View Article Online
DOI: 10.1039/C7DT02077E



attributed to the $F_{2g}$ symmetric vibration mode of the 8-fold Ce-O bond in the fluorite type structure. This vibrational mode is often used for comparison of various ceria based or related systems.[38] As mentioned earlier, $CeO_2$ can be considered as the parent structure of ME-REOs ($(RE)O_{2-\delta}$), wherein all the different RE elements substitute Ce. Thus, the $F_{2g}$ band is also observed in the Raman spectra of the ME-REOs (Figure 5). The frequency of this signal is expected to be independent of the metal identity and hence, the cation mass.[38] However, the position of the band shows a strong red shift (~15 $cm^{-1}$) for the ME-REOs with respect to $CeO_2$. Shifting of this $F_{2g}$ band along with broadening is a common feature often related[39,40] to chemical substitutions, which lead to expansion of the crystal lattices, variation in the M-O bond lengths and formation of oxygen defects. These reasons are valid for ME-REOs as well. The lattice parameter for the as-synthesized $CeO_2$ is 5.42 Å, while for all ME-REOs a relative expansion of the crystal lattice is observed, as mentioned in Section 3.3. Furthermore, it is observed that the intensity of the $F_{2g}$ band is the strongest for pure $CeO_2$ and gradually decreases with addition of more elements, for all ME-REOs, which is in good agreement with the results reported in literature.[39,41] The intensity lowering of the band is mainly related to the formation of multicomponent solid solution (consisting of various rare earth elements) in ME-REOs, which leads to symmetry breaking of the ceria lattice and hence, affects $F_{2g}$ symmetric vibration mode. Except for $CeO_2$, an additional broad band centered ~570 $cm^{-1}$ is observed for all the other systems. This band ($V_o$ in Figure 5) is related to the oxygen vacancies present in the systems.[19,32,39] The ratio of the integral intensity of the band corresponding to the oxygen vacancies ($II_{Vo}$), to the integral intensity corresponding to the $F_{2g}$ band ($II_{F2g}$) portrays the relative oxygen vacancies concentration. In some cases,[19,32] instead of a single broad band ~570 $cm^{-1}$ two separate bands (at ~550 $cm^{-1}$ and ~600 $cm^{-1}$) are observed which are also related to the

View Article Online
DOI: 10.1039/C7DT02077E



defect states. In that case, summation of the integral intensities of both defect bands are used instead of the single $II_{Vo}$ to calculate the relative oxygen vacancies concentration.[19] Although this ratio, $II_{Vo}/II_{F2g}$, does not provide a quantitative information about the amount of oxygen vacancies, it is often used as a reliable tool to compare the amount of oxygen defects present in different systems.[19,39,42]

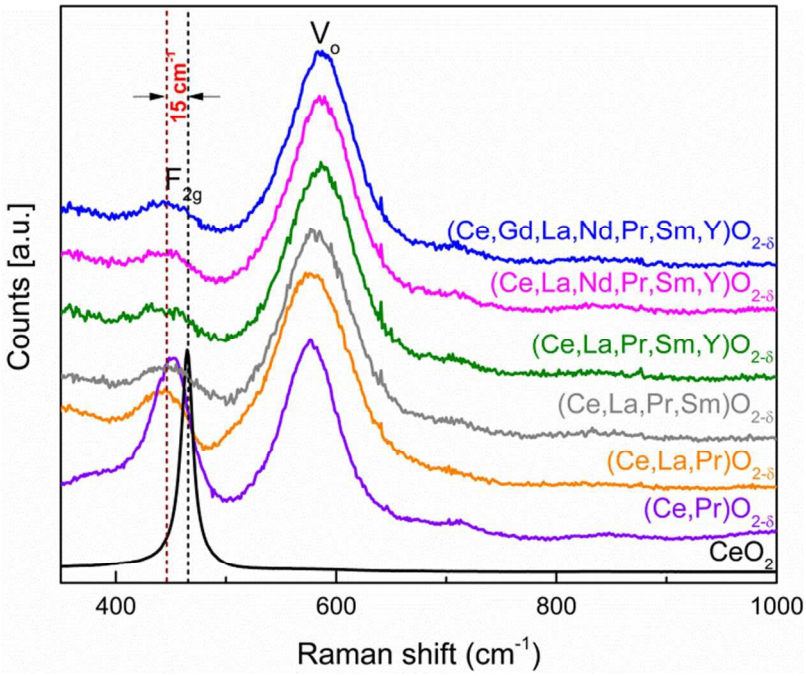


**Figure 5.** Raman spectra of pure $CeO_2$ and different ME-REOs obtained using a He-Ne laser ($\lambda$ = 633 nm). The $F_{2g}$ vibration mode for ceria lies at 465 $cm^{-1}$ whereas for the ME-REOs a red shift (~15 $cm^{-1}$) is observed. An additional broad band (~570 $cm^{-1}$) is observed for all the ME-REOs, which is related to the oxygen vacancies (*Vo*) present in the structure.

Figure 6 displays the amount of oxygen vacancies ($\delta$) calculated from the charge balance approach (see Table 2 and Equation 4) as well as the relative oxygen vacancies concentration ($II_{Vo}/II_{F2g}$) obtained from the Raman spectra for different ME-REOs. The relative oxygen vacancies concentration obtained from Raman spectroscopy shows a rapid increase with the increase in the number of elements. It then saturates when the number of elements becomes

View Article Online
DOI: 10.1039/C7DT02077E



higher than 6. This variation follows a trend similar to the variation of amount of the oxygen vacancies ($\delta$) calculated from the charge balance equation using the XPS and the UV-Vis data.

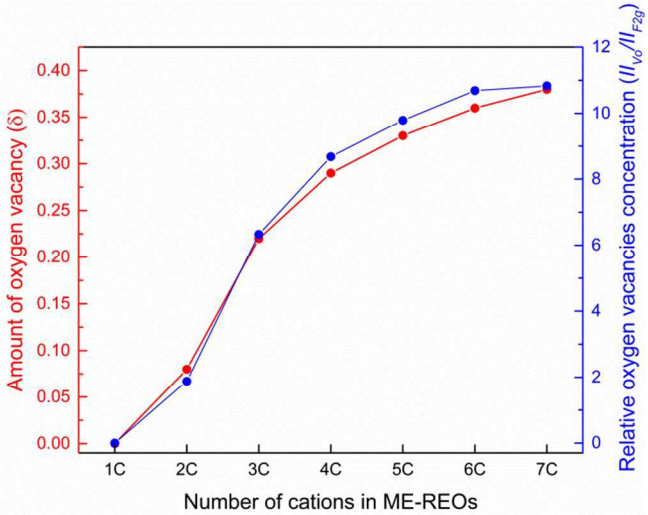


**Figure 6**. Comparison of the amount of oxygen vacancies ($\delta$) calculated from the charge balance equation (see Equation 4) and the relative oxygen vacancies concentration estimated from the Raman spectra ($II_{Vo}/II_{F2g}$), as a function of number of cations in ME-REOs, where 1C = $CeO_2$, 2C = $(Ce,Pr)O_{2-\delta}$, 3C = $(Ce,La,Pr)O_{2-\delta}$, 4C = $(Ce,La,Pr,Sm)O_{2-\delta}$, 5C = $(Ce,La,Pr,Sm,Y)O_{2-\delta}$, 6C = $(Ce,La,Nd,Pr,Sm,Y)O_{2-\delta}$ and 7C = $(Ce,Gd,La,Nd,Pr,Sm,Y)O_{2-\delta}$.

**3.5. Possible reasons for the band gap narrowing.** The narrowing of the band gap, in several systems,[43–45] is often related to the formation of intermediate energy states due to the presence of point defects, like oxygen vacancies. The same is likely true for ME-REOs, especially considering the high amount of oxygen vacancies present in these systems. Interestingly, the change in the band gap values in ME-REOs is not directly related to the change in the amount of oxygen vacancies (compare Table 1 and 2). Furthermore, in oxide systems, like $CeO_2$ or $TiO_2$, where oxygen vacancies are often identified as the reason for the band gap narrowing, a decrease of band gap energy by only 0.32 eV[46] or 0.30 eV,[44] respectively, is observed. However, considering $CeO_2$ as the parent structure of ME-REOs, the extent of the

View Article Online
DOI: 10.1039/C7DT02077E

band gap narrowing in ME-REOs is more than 1 eV, which indicates that some additional factors other than oxygen vacancies are likely involved in the band gap narrowing.

The presence of certain multivalent elements is known to have a strong impact on the band gap, and hence, the light absorption behavior, in some systems, like Cu doped ZnO[14] and Pr doped $CeO_2$.[21] In case of ME-REOs the presence of Pr in a multivalent state can be one of the reasons for the observed band gap narrowing. To ensure the validity of this reasoning three different ME-REO systems without Pr (i.e., $(Ce,La,Sm)O_{2-\delta}$, $(Ce,La,Sm,Y)O_{2-\delta}$ and $(Ce,La,Nd,SmY)O_{2-\delta}$) are synthesized. The XRD analysis (see Supplementary Information Figure S2-a and related discussion) show that these systems are phase pure and also have a fluorite type of structure just like the ME-REOs with Pr. However, the band gap values (see Supplementary Information Figure S2b) of these three ME-REO systems (without Pr) are in the range of 2.90 – 3.05 eV, i.e., around 1 eV higher than the ME-REO systems with Pr. The band gap values of these three systems are also close to that of $CeO_2$ (3.2 eV) and the small difference in the values (0.30 – 0.15 eV) is related to the oxygen defects present in the systems. Hence, it is concluded that Pr plays a dominant role in the band gap narrowing of ME-REOs.

Based on these results, a possible schematic of the band structure of ME-REOs (Figure 7) is discussed in the following lines. In rare earth oxides, most of the RE elements have their O 2*p* and RE 5*d* energy levels at relatively similar positions. However, the position of occupied and unoccupied RE 4*f* energy bands, which are located in between O 2*p* and RE 5*d* energy bands, plays a crucial role in determining the type of electronic transition and, therefore, the band gap value. In most of the RE sesquioxides, the band gap values are related to electronic transitions from O 2*p* to RE 5*d* or $5d + 4f_{\text{unoccupied}}$ energy bands (as in $La_2O_3$ or $Sm_2O_3$, respectively) [47], as shown in Figure 7, case I. The $5d + 4f_{\text{unoccupied}}$ is relevant for those lanthanides whose unoccupied

View Article Online
DOI: 10.1039/C7DT02077E



4*f* bands fall into the 5*d* energy band.[47] The electronic transitions in case of $CeO_2$ occurs from O 2*p* to Ce 4*f* energy level (see Figure 7, case II) and these transition are activated due to the inherent oxygen vacancies present in ceria.[47,48] In ME-REOs without Pr, the electronic transitions are possibly very similar to that in ceria, while the presence of oxygen vacancies might have narrowed down the gap between the O 2*p* and Ce 4*f* energy level (see Figure 7, case III). In Pr substituted $CeO_2$ systems, it is believed that an additional Pr 4*f* band, between the O 2*p* and Ce 4*f*, is present.[49] The same is likely to be true for ME-REOs with Pr. Thus, the band gap of ~2 eV in ME-REOs with Pr can be related to the electronic transition between the O 2*p* to Pr 4*f* , which lies ~1 eV[49] below the Ce 4*f* energy band (see Figure 7, case IV).

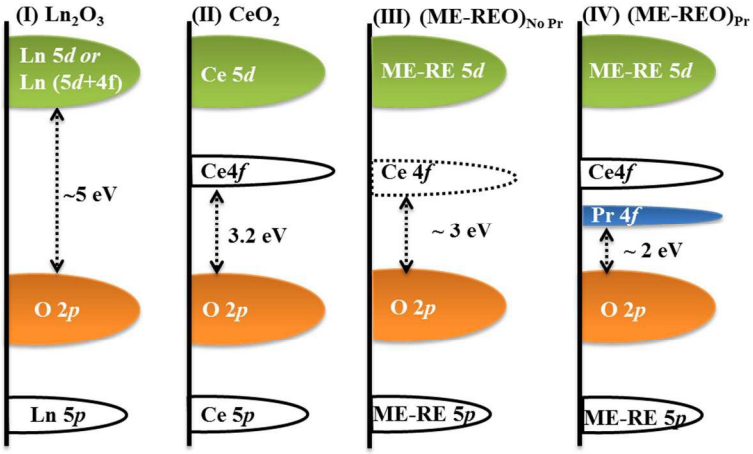


**Figure 7**. Schematic of band structures of $Ln_2O_3$, where Ln = $Gd^{3+}$, $La^{3+}$, $Sm^{3+}$, etc. (case I), $CeO_2$ (case II), ME-REOs without Pr (case III) and ME-REOs with Pr (case IV), depicting the possible mechanism for band gap narrowing.

## 4. CONCLUSIONS

In this work, newly discovered multicomponent equiatomic rare oxides (ME-REOs) are investigated using a combination of diffraction and spectroscopic techniques. The results show that while Ce has a strong impact on the crystal structure and phase purity of the ME-REOs, their optical properties are related to the presence of multivalent Pr. The band gap energies of ME-

View Article Online
DOI: 10.1039/C7DT02077E



REOs containing Pr are in the range of 1.95 – 2.14 eV, enabling light absorption over the entire visible spectral range. The presence of rare earth (RE) cations in oxidation states other than 4+ results in the formation of oxygen vacancies in the ME-REOs, which is confirmed by Raman spectroscopy. A combination of Ce and Pr in the ME-REO systems helps to achieve both phase purity and lower band gap, which are largely independent of the other RE cations present. This provides great flexibility for engineering the amount of defects (oxygen vacancies) or/and allows element based property tuning (by adding the required cations) without compromising the phase purity or the visible light absorbing capability of ME-REOs. Further studies on ME-REOs are likely to focus on visible light absorption and oxygen vacancy related research and applications. In parallel, theoretical studies to model the electronic structure of these new oxides will be very helpful.

**Notes**

The authors declare no competing financial interest.

**ACKNOWLEDGMENT**

The authors would like to thank the Helmholtz Association (Germany) for financial support through the Helmholtz Portfolio Project “Electrochemical Storage in Systems - Reliability and Integration”, Prof. Dr. Heinz von Seggern and Elmar Kersting (Technische Universität Darmstadt, Germany) for providing access to the UV-Vis spectrophotometer, Prof. Dr. Oliver Clemens and Prof. Dr. Christian Hess (Technische Universität Darmstadt, Germany) for fruitful discussions. Leonardo Velasco thanks Karlsruhe Nano Micro Facility (KNMF, Germany) and Dr. Christian Kübel for providing access to TEM at KIT. Tiju Thomas thanks the Department of Science and Technology, Government of India for financial support through projects (DST FILE NO. YSS/2015/001712 and DST 11-IFA-PH-07), and the Fast Track Young Scientist Award.

View Article Online
DOI: 10.1039/C7DT02077E



## REFERENCES

1 C. M. Rost, E. Sachet, T. Borman, A. Moballegh, E. C. Dickey, D. Hou, J. L. Jones, S. Curtarolo and J.-P. Maria, *Nat. Commun.*, 2015, **6**, 8485.

2 D. Bérardan, S. Franger, D. Dragoe, A. K. Meena and N. Dragoe, *Phys. status solidi - Rapid Res. Lett.*, 2016, **10**, 328–333.

3 D. Bérardan, S. Franger, A. K. Meena and N. Dragoe, *J. Mater. Chem. A*, 2016, **4**, 9536–9541.

4 Z. Rak, C. M. Rost, M. Lim, P. Sarker, C. Toher, S. Curtarolo, J.-P. Maria and D. W. Brenner, *J. Appl. Phys.*, 2016, **120**, 95105.

5 A. Sarkar, R. Djenadic, N. J. Usharani, K. P. Sanghvi, V. S. K. Chakravadhanula, A. S. Gandhi, H. Hahn and S. S. Bhattacharya, *J. Eur. Ceram. Soc.*, 2017, **37**, 747–754.

6 B. S. Murty, J. W. Yeh and S. Ranganathan, *High-Entropy Alloys*, Butterworth-Heinemann, London, 2014.

7 R. Djenadic, A. Sarkar, O. Clemens, C. Loho, M. Botros, V. S. K. Chakravadhanula, C. Kübel, S. S. Bhattacharya, A. S. Gandhi and H. Hahn, *Mater. Res. Lett.*, 2017, **5**, 102–109.

8 S. J. Schneider and R. S. Roth, *J. Res. Natl. Bur. Stand. Sect. A Phys. Chem.*, 1960, **64A**, 317.

9 G. Adachi, N. Imanaka and Z. C. Kang, *Binary Rare Earth Oxides*, Kluwer Academic Publishers, Dordrecht, 2005.

View Article Online
DOI: 10.1039/C7DT02077E



10 A. M. D'Angelo, A. C. Y. Liu and A. L. Chaffee, *J. Phys. Chem. C*, 2016, **120**, 14382–14389.

11 M. Balaguer, C. Solís, S. Roitsch and J. M. Serra, *Dalt. Trans.*, 2014, **43**, 4305–4312.

12 C. Mao, Y. Zhao, X. Qiu, J. Zhu and C. Burda, *Phys. Chem. Chem. Phys.*, 2008, **10**, 5633.

13 S. Kumar, A. K. Ojha, D. Patrice, B. S. Yadav and A. Materny, *Phys. Chem. Chem. Phys.*, 2016, **18**, 11157–11167.

14 N. Mary Jacob, G. Madras, N. Kottam and T. Thomas, *Ind. Eng. Chem. Res.*, 2014, **53**, 5895–5904.

15 A. Chaudhary, M. P. Nag, N. Ravishankar, T. Thomas, M. Jain and S. Raghavan, *J. Phys. Chem. C*, 2014, **118**, 29788–29795.

16 *Topas V5, General profile and structure analysis software for powder diffraction data, User's Manual*, Bruker AXS, Karlsruhe, Germany, 2015.

17 J. Tauc, R. Grigorovici and A. Vancu, *Phys. Status Solidi*, 1966, **15**, 627–637.

18 A. Machocki, T. Ioannides, B. Stasinska, W. Gac, G. Avgouropoulos, D. Delimaris, W. Grzegorczyk and S. Pasieczna, *J. Catal.*, 2004, **227**, 282–296.

19 M. Guo, J. Lu, Y. Wu, Y. Wang and M. Luo, *Langmuir*, 2011, **27**, 3872–3877.

20 P. De Rouffignac, J. Park and R. G. Gordon, *Chem. Mater.*, 2005, **17**, 4808–4814.

21 K. Ahn, D. S. Yoo, D. H. Prasad, H. W. Lee, Y. C. Chung and J. H. Lee, *Chem. Mater.*, 2012, **24**, 4261–4267.

View Article Online
DOI: 10.1039/C7DT02077E



22 J. P. Holgado, R. Alvarez and G. Munuera, *Appl. Surf. Sci.*, 2000, **161**, 301–315.

23 S. Lütkehoff, M. Neumann and A. Ślebarski, *Phys. Rev. B*, 1995, **52**, 13808–13811.

24 I. Tankov, B. Pawelec, K. Arishtirova and S. Damyanova, *Appl. Surf. Sci.*, 2011, **258**, 278–284.

25 M. Balestrieri, S. Colis, M. Gallart, G. Schmerber, M. Ziegler, P. Gilliot and A. Dinia, *J. Mater. Chem. C*, 2015, **3**, 7014–7021.

26 N. Rakov and G. S. Maciel, *J. Mater. Chem. C*, 2016, **4**, 5442–5447.

27 N. Shasmal, P. K and B. Karmakar, *RSC Adv.*, 2015, **5**, 81123–81133.

28 S. Omar, E. D. Wachsman and J. C. Nino, *Solid State Ionics*, 2008, **178**, 1890–1897.

29 T. M. Inerbaev, A. S. Karakoti, S. V. N. T. Kuchibhatla, A. Kumar, A. E. Masunov and S. Seal, *Phys. Chem. Chem. Phys.*, 2015, **17**, 6217–6221.

30 Z. C. Orel and B. Orel, *Phys. Status Solidi B*, 1994, **186**, K33–K36.

31 S. Tsunekawa, T. Fukuda and A. Kasuya, *J. Appl. Phys.*, 2000, **87**, 1318.

32 A. Filtschew, K. Hofmann and C. Hess, *J. Phys. Chem. C*, 2016, **120**, 6694–6703.

33 A. V. Prokofiev, A. I. Shelykh and B. T. Melekh, *J. Alloys Compd.*, 1996, **242**, 41–44.

34 G. Adachi and N. Imanaka, *Chem. Rev.*, 1998, **98**, 1479–1514.

35 S. Zinatloo-Ajabshir and M. Salavati-Niasari, *New J. Chem.*, 2015, **39**, 3948–3955.

36 Y.-N. Xu, Z. Gu and W. Y. Ching, *Phys. Rev. B*, 1997, **56**, 14993–15000.

View Article Online
DOI: 10.1039/C7DT02077E



37 Z. Wang, Z. Quan and J. Lin, *Inorg. Chem.*, 2007, **46**, 5237–5242.

38 C. Artini, M. Pani, M. M. Carnasciali, M. T. Buscaglia, J. R. Plaisier and G. A. Costa, *Inorg. Chem.*, 2015, **54**, 4126–4137.

39 N. Paunović, Z. Dohčević-Mitrović, R. Scurtu, S. Aškrabić, M. Prekajski, B. Matović and Z. V. Popović, *Nanoscale*, 2012, **4**, 5469.

40 B. M. Reddy, G. Thrimurthulu, L. Katta, Y. Yamada and S.-E. Park, *J. Phys. Chem. C*, 2009, **113**, 15882–15890.

41 A. Dubey, S. K. Kolekar and C. S. Gopinath, *ChemCatChem*, 2016, **8**, 3650–3656.

42 A. S. Babu, R. Bauri and G. S. Reddy, *Electrochim. Acta*, 2016, **209**, 541–550.

43 J. Wang, Z. Wang, B. Huang, Y. Ma, Y. Liu, X. Qin, X. Zhang and Y. Dai, *ACS Appl. Mater. Interfaces*, 2012, **4**, 4024–4030.

44 A. K. Rumaiz, J. C. Woicik, E. Cockayne, H. Y. Lin, G. H. Jaffari and S. I. Shah, *Appl. Phys. Lett.*, 2009, **95**, 262111.

45 B. Huang, R. Gillen and J. Robertson, *J. Phys. Chem. C*, 2014, **118**, 24248–24256.

46 S. A. Ansari, M. M. Khan, M. O. Ansari, S. Kalathil, J. Lee and M. H. Cho, *RSC Adv.*, 2014, **4**, 16782.

47 R. Gillen, S. J. Clark and J. Robertson, *Phys. Rev. B*, 2013, **87**, 125116.

48 C. W. M. Castleton, J. Kullgren and K. Hermansson, *J. Chem. Phys.*, 2007, **127**, 244704.

49 J. J. Kim, S. R. Bishop, D. Chen and H. L. Tuller, *Chem. Mater.*, 2017, **29**, 1999–2007.

View Article Online
DOI: 10.1039/C7DT02077E



**Table of contents entry**

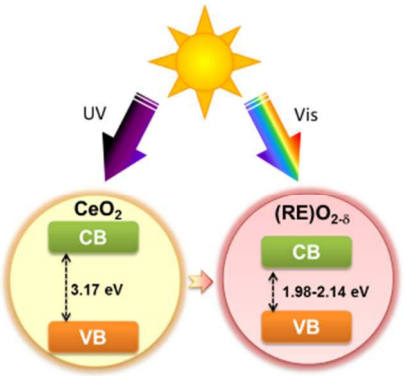


**Synopsis**

Phase pure multinary rare earth oxides, containing multivalent praseodymium, have narrow band gap and high level of oxygen vacancies.